NASA/CR—2006-214338 EDR–90712

Spin Testing of Superalloy Disks With Dual Grain Structure

Tab M. Heffernan
Rolls-Royce North American Technologies, Inc., Indianapolis, Indiana

May 2006

NASA STI Program . . . in Profile

Since its founding, NASA has been dedicated to the advancement of aeronautics and space science. The NASA Scientific and Technical Information (STI) program plays a key part in helping NASA maintain this important role.

The NASA STI Program operates under the auspices of the Agency Chief Information Officer. It collects, organizes, provides for archiving, and disseminates NASA's STI. The NASA STI program provides access to the NASA Aeronautics and Space Database and its public interface, the NASA Technical Reports Server, thus providing one of the largest collections of aeronautical and space science STI in the world. Results are published in both non-NASA channels and by NASA in the NASA STI Report Series, which includes the following report types:

- TECHNICAL PUBLICATION. Reports of completed research or a major significant phase of research that present the results of NASA programs and include extensive data or theoretical analysis. Includes compilations of significant scientific and technical data and information deemed to be of continuing reference value. NASA counterpart of peer-reviewed formal professional papers but has less stringent limitations on manuscript length and extent of graphic presentations.

- TECHNICAL MEMORANDUM. Scientific and technical findings that are preliminary or of specialized interest, e.g., quick release reports, working papers, and bibliographies that contain minimal annotation. Does not contain extensive analysis.

- CONTRACTOR REPORT. Scientific and technical findings by NASA-sponsored contractors and grantees.

- CONFERENCE PUBLICATION. Collected papers from scientific and technical conferences, symposia, seminars, or other meetings sponsored or cosponsored by NASA.

- SPECIAL PUBLICATION. Scientific, technical, or historical information from NASA programs, projects, and missions, often concerned with subjects having substantial public interest.

- TECHNICAL TRANSLATION. English-language translations of foreign scientific and technical material pertinent to NASA's mission.

Specialized services also include creating custom thesauri, building customized databases, organizing and publishing research results.

For more information about the NASA STI program, see the following:

- Access the NASA STI program home page at *http://www.sti.nasa.gov*

- E-mail your question via the Internet to *help@sti.nasa.gov*

- Fax your question to the NASA STI Help Desk at 301–621–0134

- Telephone the NASA STI Help Desk at 301–621–0390

- Write to:
  NASA STI Help Desk
  NASA Center for AeroSpace Information
  7121 Standard Drive
  Hanover, MD 21076–1320

NASA/CR—2006-214338 EDR–90712

Spin Testing of Superalloy Disks With Dual Grain Structure

Tab M. Heffernan
Rolls-Royce North American Technologies, Inc., Indianapolis, Indiana

Prepared under Contract NAS3–01143, Task 4

National Aeronautics and
Space Administration

Glenn Research Center
Cleveland, Ohio 44135

May 2006

Level of Review: This material has been technically reviewed by NASA technical management.

Available from

NASA Center for Aerospace Information
7121 Standard Drive
Hanover, MD 21076–1320

National Technical Information Service
5285 Port Royal Road
Springfield, VA 22161

Available electronically at http://gltrs.grc.nasa.gov

Contents

List of Figures

List of Tables

1.0 Introduction

This 24-month program was a joint effort between Allison Advanced Development Company (AADC), General Electric Aircraft Engines (GEAE), and NASA Glenn Research Center (GRC). AADC led the disk and spin hardware design and analysis utilizing existing Rolls-Royce turbine disk forging tooling. Testing focused on spin testing four disks: two supplied by GEAE and two by AADC. The two AADC disks were made of Alloy 10, and each was subjected to a different heat treat process: one producing dual microstructure with coarse grain size at the rim and fine grain size at the bore and the other produced single fine grain structure throughout. The purpose of the spin tests was to provide data for evaluation of the impact of dual grain structure on disk overspeed integrity (yielding) and rotor burst criteria. The program culminated with analysis and correlation of the data to current rotor overspeed criteria and advanced criteria required for dual structure disks.

1.1 Program Objectives

The prime objective of this program was to demonstrate that yield and burst behavior of dual structure disks can be predicted accurately. The program was organized into the following, separately funded and evaluated, work elements (WE):

- WE 1—Define disk geometry, alloy, and heat treat
- WE 2—Disk machining, instrumentation, and spin test definition
- WE 3—Characterize static and cyclic disk behavior and predict spin pit behavior of disks
- WE 4—Analyze spin test data

NOTE: NASA GRC was responsible for all aspects of the actual spin test.

1.2 Program Plan

AADC and GEAE worked together to conduct the following orderly structured tasks to enable spin testing of four superalloy disks with dual grain structure:

- Design the configuration for the disks and the spin pit adaptive hardware and procure uniform and dual grain structure disks
- Provide baseline and dual heat treated Alloy 10 and René 104 forgings machined to the identified spin test disk geometry

- Define, but not perform, spin test experiments to generate data permitting verification of sizing methodologies pertinent to advanced subsonic turbine engines (spin test experiments were separately funded by NASA at Test Devices, Inc.)
- Predict spin pit behavior of four disks using GEAE and AADC/Rolls-Royce conventional and advanced methodologies
- Compare predicted versus demonstrated behavior of dual grain structure versus baseline material
- Prepare a final report documenting the results of all program tasks

2.0 Details of Work Accomplished

2.1 WE 1—Define Disk Geometry, Alloy, and Heat Treat

2.1.1 Define Disk Geometry

AADC had the lead for disk sizing and design, but the effort was accomplished with GEAE cooperation and concurrence. Existing tooling was used to forge the disk because it provided:

- Convenient size for spin pit testing
- Used in previous DMHT development projects funded by NASA, so processing relating to the DMHT process was already available
- Available for use at no cost

The spin test disk was designed to match the radial, tangential, and equivalent stress distribution of the production turbine disk. The final design included 36 equally spaced holes in the wheel rim (Figure 1). Through-cuts were placed top dead center on each rim hole, thus shifting the last continuous fiber of the wheel from the outside diameter to the base of the rim holes. This isolated the mass between each hole. This ‘dead weight’ was designed into the disk to simulate the effect of a blade load for the spin test.

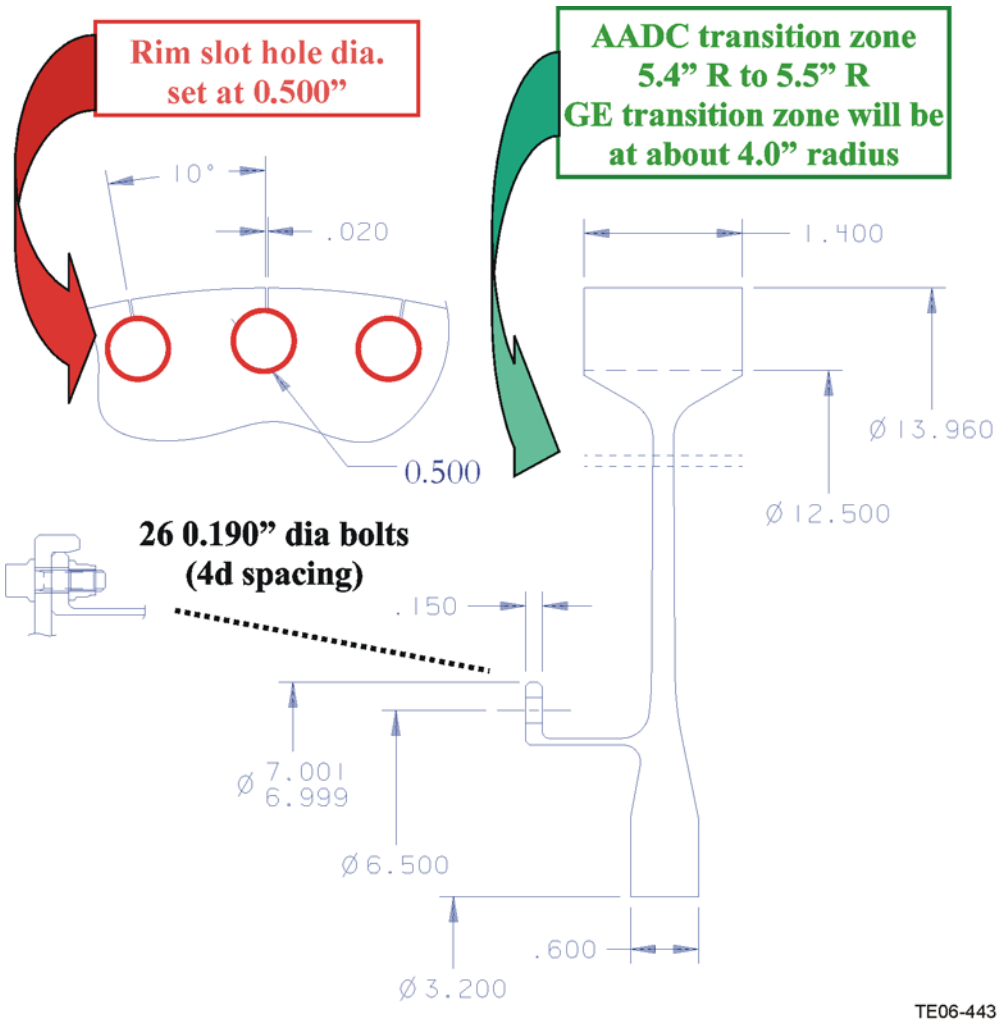

Figure 1. Disk Design.

A three-dimensional (3-D) finite element analysis (FEA) was performed on a 10-deg sector of the AADC prototype turbine disk (Figure 2). The analysis also included the spin arbor that was modeled using a tied contact assumption as opposed to actually modeling the bolted joint. ABAQUS 6.4.2 was used as the finite element solver.

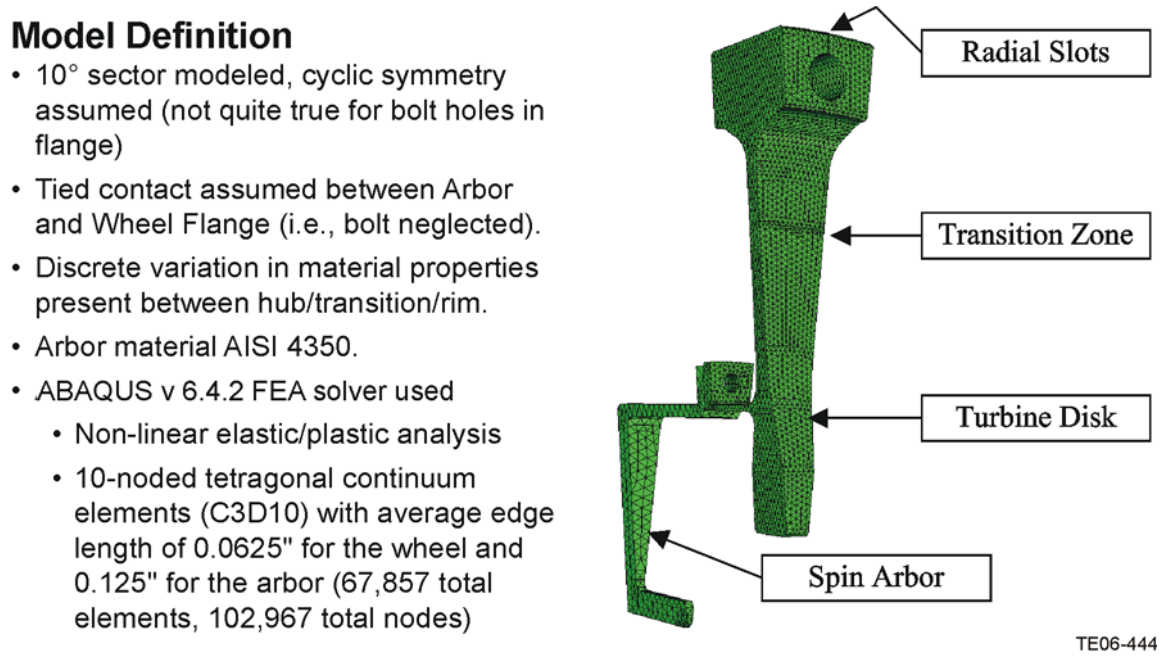

Figure 2. Disk and Arbor Finite Element Analysis.

The spin test was modeled using both linear elastic and elastic-plastic constitutive behaviors. Ten-noded tetragonal continuum elements (C3D10) were used to model both the arbor and the wheel. The final model contained 67,857 elements and 102,967 nodes. The average element edge length for the disk was 0.0625 and 0.125 in. for the arbor. The nonlinear elastic-plastic behavior was modeled by including tabular input of the true stress-logarithmic strain response of the material obtained from representative smooth bar tensile tests.

The initial AADC design incorporated 0.120-in. diameter through-holes at the bottom of the rim slots. GEAE analysis indicated the through-hole should be 0.500-in. diameter as shown in Figure 1. AADC analysis showed burst rpm would increase from the initially proposed 0.120-in. diameter due to material reduction, but would still remain within spin pit drive motor capability.

2.1.2 Additional Analysis Due to Machining Error

An instrumentation hole was mistakenly machined into the wheel flange arm—0.0625-in. diameter located 0.46 in. axially from the inside of the wheel flange face (Figure 3).

AADC performed an analysis to determine whether failure of the initiation site could move from the intended location at the rim hole to the instrumentation hole. The presence of the hole would produce a K_t of 3.0 if the material were operating in a linear elastic regime. Under the intended test plan loading, plasticity would allow local yielding and load redistribution near the hole. To

determine the resulting stress and strain present in the vicinity of the hole, the hole geometry was added to a 10-deg sector of the wheel/arbor assembly, and a nonlinear elastic/plastic FEA was performed. Peak strains and stresses near the hole were compared to those in the intended failure region. A slotted-hole geometry was also analyzed. The slot had a 4:1 ratio between the run and the end diameters. This resulted in a K_t of approximately 1.75. A 30-deg sector model was used to provide enough material on either end of the slot to reach far-field values before encountering the symmetry plane. Peak strains and stresses were again compared to those in the intended failure region as well as those for the round hole (Figures 3 and 4).

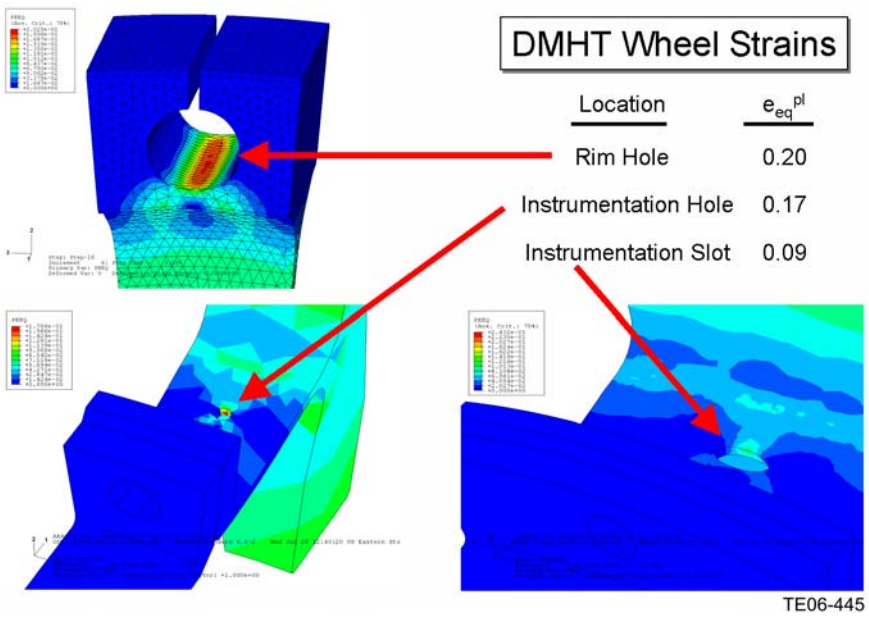

Figure 3. Disk Strains with Instrumentation Hole.

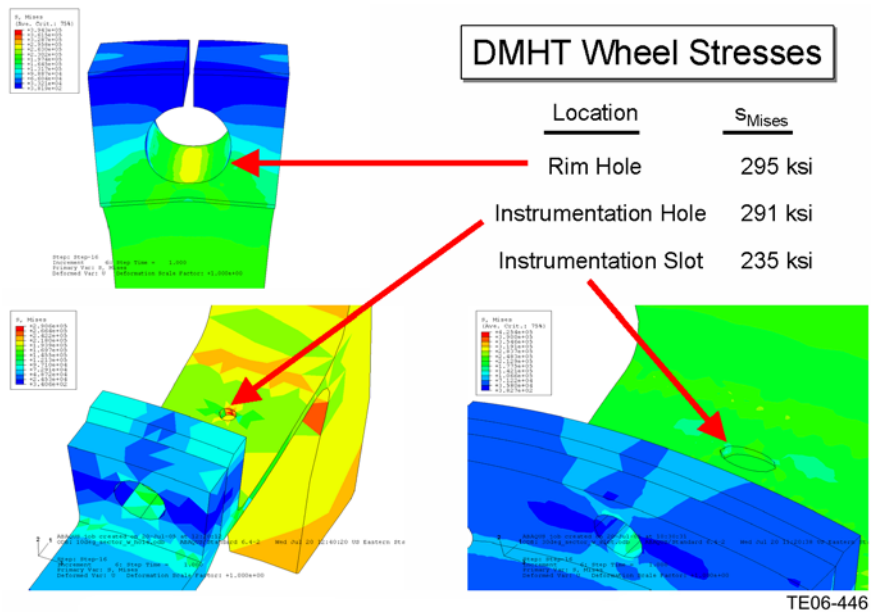

Figure 4. Disk Stresses with Instrumentation Hole.

While the peak strain remained at the rim hole for both considered geometries, the magnitudes at the instrumentation hole approached the rim hole values for the round hole case. Values were significantly reduced for the slotted geometry. These values are listed in Table 1. As a result of the analysis predictions, it was recommended that the instrumentation holes in both the DMHT and subsolvus wheels be remachined into a slotted geometry with a 4:1 length-to-diameter ratio.

TABLE 1. SUMMARY OF STRAINS/STRESSES AT CRITICAL AREAS AS A FUNCTION OF WHEEL SPEED.

		Hole			Slot			Rim Hole	
RPM		ε_{eq}^{pl}	σ_{Mises} [ksi]		ε_{eq}^{pl}	σ_{Mises} [ksi]		ε_{eq}^{pl}	σ_{Mises} [ksi]
24500		0.065	218		0.025	183		0.085	221
25000		0.105	247		0.040	194		0.126	247
25500		0.140	274		0.055	205		0.166	288
26000		0.170	291		0.090	235		0.200	295

2.1.3 Alloy Selection and Heat Treat Definition

AADC/Rolls-Royce selected Alloy 10 for the forging material and NASA's patented DMHT process for producing the dual microstructure forgings. The Alloy 10 composition selected represents Honeywell Energy Systems' recent improvements to this alloy to enhance fatigue strength while maintaining the alloy's superior creep resistance. The Alloy 10 forging stock was delivered at no cost by Rolls-Royce. Ladish Company, Inc. produced three forgings from this

material using isothermal forging tooling for an existing Rolls-Royce turbine wheel. The forgings were produced using parameters previously developed by Ladish and Rolls-Royce.

All three forgings were near-solvus solution heat treated to achieve a target grain size of ASTM 10-13. One forging was cooled from solution heat treatment using Ladish's Supercool™ cooling technology under controlled conditions to represent cooling rates typical for large civil engine disk bores. Finite element modeling was conducted by Ladish on a parallel program funded by Rolls-Royce plc. to determine the Supercooler parameter settings and validate achievement of the target cooling rates. The other two forgings were conventionally fan air cooled in preparation for DMHT processing.

The DMHT technique is a NASA patented method for the development of a dual microstructure disk component. The DMHT specific setup employed for this disk shape and program effort is shown in Figure 5. This DMHT tooling was the same tooling that was previously used to produce Rolls-Royce production turbine wheel DMHT forgings using alloys ME209 and LSHR under NASA funding. The disk component with the surrounding insulation packages was placed into a furnace operating at a supersolvus temperature. This practice enabled the rim section to heat above the gamma prime solvus and elicit a grain coarsened response, while the bore (inside the insulation package) remained subsolvus and retained the original grain size.

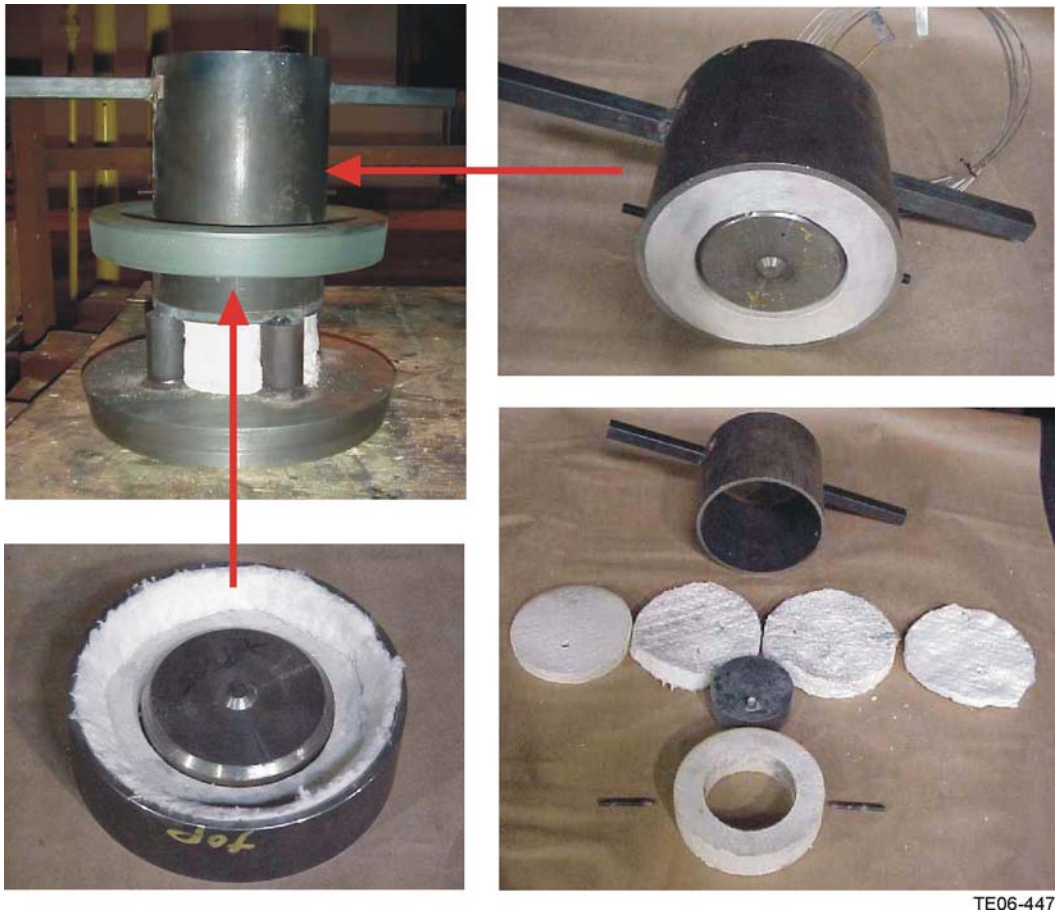

Figure 5. DMHT Heating Setup; AE 2100, Stage 3 Disk.

The hold time for the DMHT treatment was selected based on thermal modeling performed by NASA and instrumented DMHT tests previously conducted using the ME209 and LSHR forgings. The NASA modeling results are illustrated in Figure 2. The design studies conducted by AADC indicated that the coarse to fine grain transition should be in the disk web about 5.4 to 5.5 inches from the centerline as illustrated in Figure 6. The team agreed by consensus to bias the aim transition zone location to the short side, i.e., nearer to the bore, to ensure that well-developed coarse grain and transition zones were achieved. Based on these criteria, a dwell time of 65 minutes at 2200°F was selected for the DMHT solutioning cycle. After heating for the 65 minutes the disk and top insulation package were removed from the furnace, leaving the bottom insulation package behind, and transferred to the Supercooler cooling station. Immediately after placing the disk at the Supercooler station, the top insulation package was quickly removed and the cooling in the Supercooler fixture was initiated using the same cooling air settings that were employed for the near-solvus processed forging.

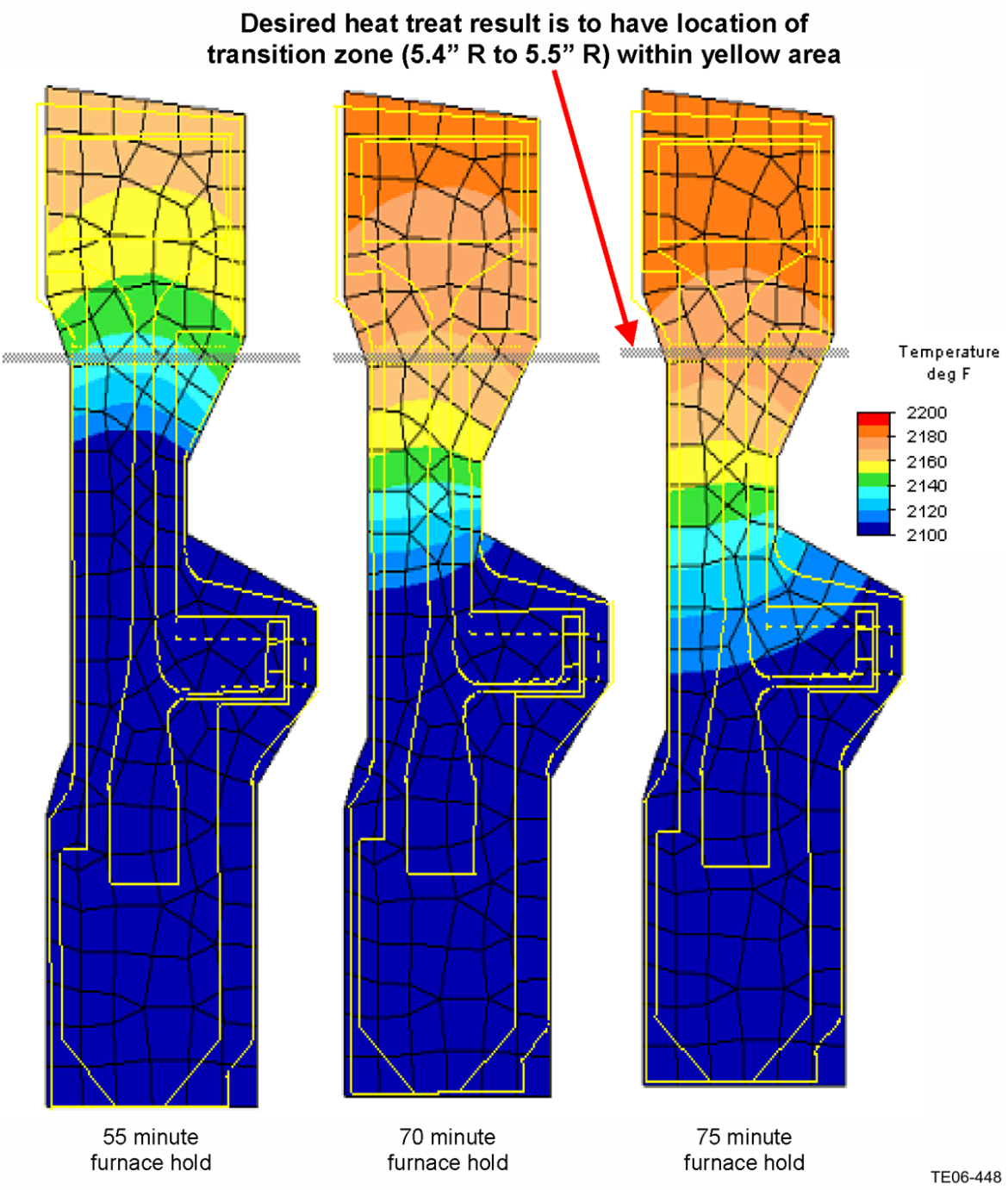

Figure 6. NASA’s Modeling Results for DMHT Processed Alloy 10 with Three Different Furnace Hold Times. Final Disk Geometry and Square-Cut Outlines are Superimposed on the Isotherm Contour Plots.

After solution heat treatment, all three forgings received a final age of 16 hours at 1400°F. The subsolvus forging and one of the two DMHT forgings were machined and inspected in accordance with drawing requirements. Both forgings met sonic inspection requirements. The DMHT forging was again sonically inspected, using higher gain and altered near-surface gating

to enable a vivid coarse-to-fine grain transition. These C-scan images are shown in Figure 7. The fine-to-coarse grain transition occurred over a narrow distance and was centered approximately 5.25 inches from the bore. This is in excellent agreement with the 5.4 to 5.5-in. target transition zone considering the intended bias towards the bore side. After ultrasonic testing, the two forgings were etched and fluorescent penetrant inspection (FPI) examined in accordance with drawing requirements. Figure 8 shows representative photographs of the etched dual microstructure forging, serial 11. These two forgings were delivered to GEAE for machining to the spin test configuration.

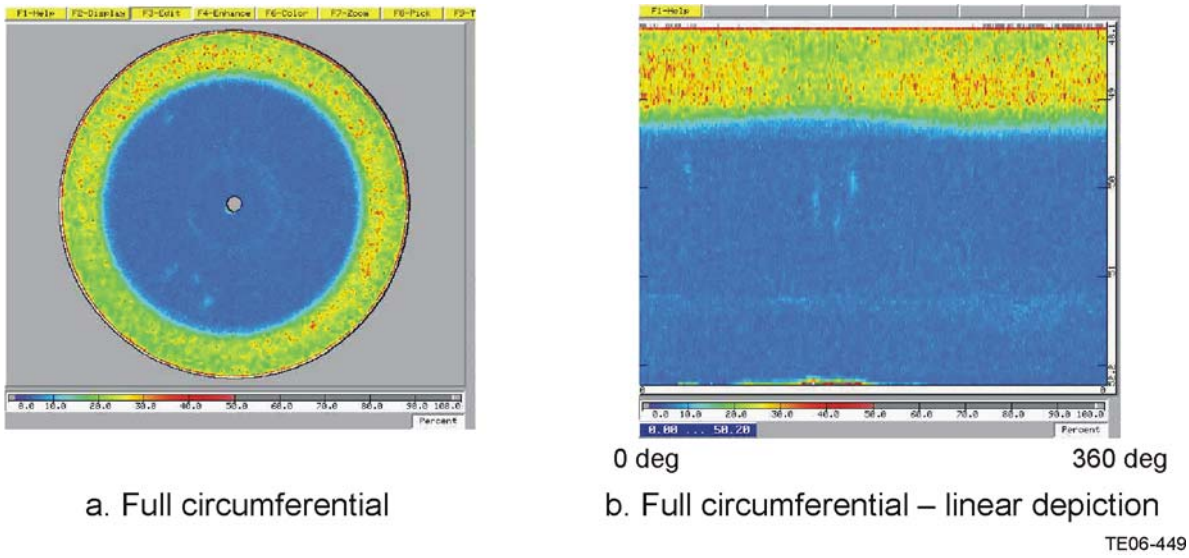

Figure 7. C-Scan Images of DMHT Processed Alloy 10 Forging.

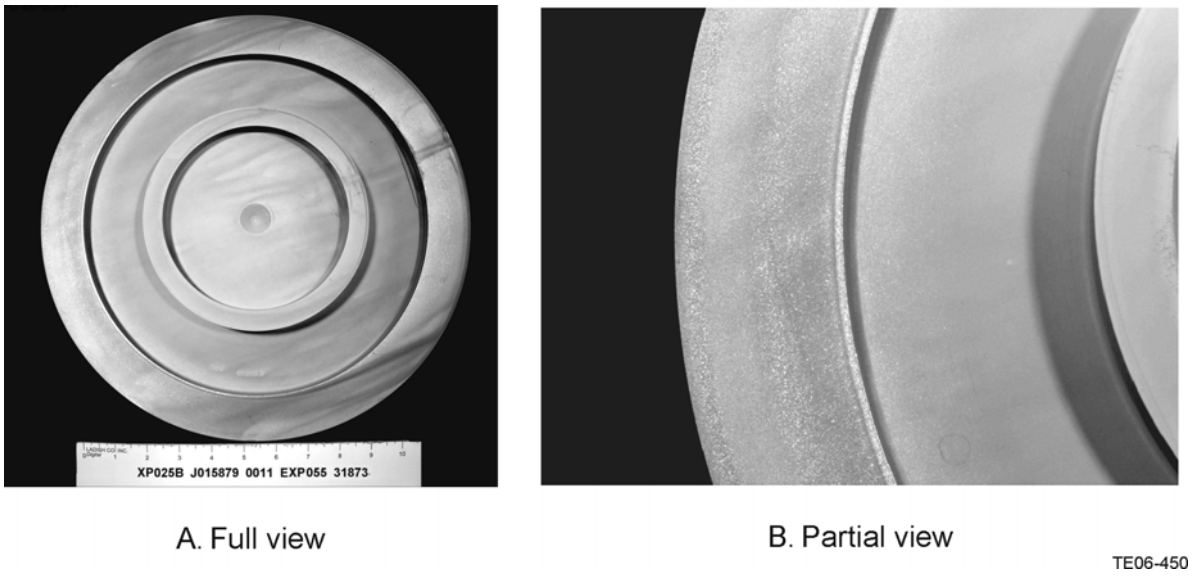

Figure 8. Representative Photographs of DMHT Processed Alloy 10 Forging.

The remaining DMHT forging was sectioned for macroetching and subsequently used by Rolls-Royce for mechanical testing. Figure 9 shows the cross-sectional macrostructure of this forging, and Figure 10 shows a closer view of the macrostructure in the fine-to-coarse grain transition zone.

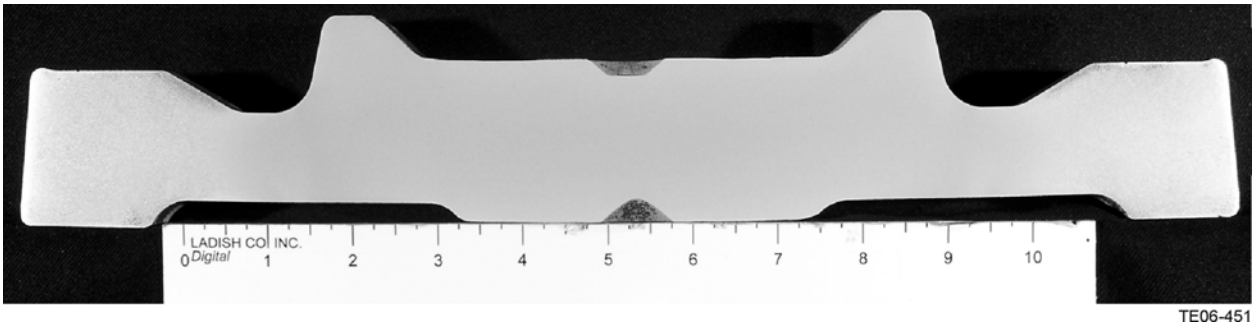

Figure 9. Macroetched Cross Section of a DMHT Processed Alloy 10 Forging.

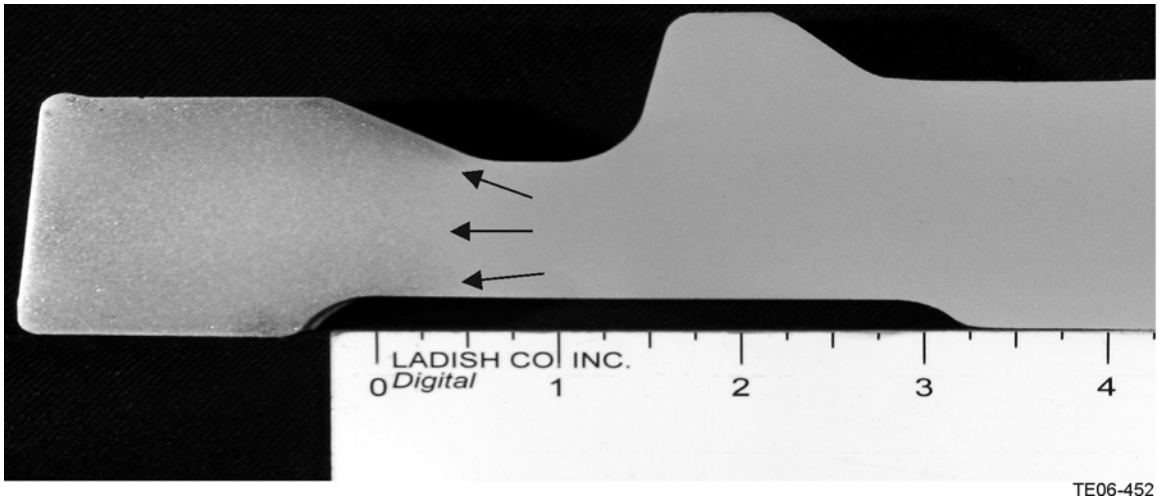

Figure 10. A Closer View of the Transition Zone in the Forging Section Shown in Figure 9.

Portions of the DMHT disk were sectioned and examined for microstructural response of the process. Figure 11 shows microstructures of web, rim, and transition zone. Grain size ranged from ASTM 10-11 in the web to ASTM 6 ala 4 in the rim. The transition zone contained a range of grain sizes from fine to coarse.

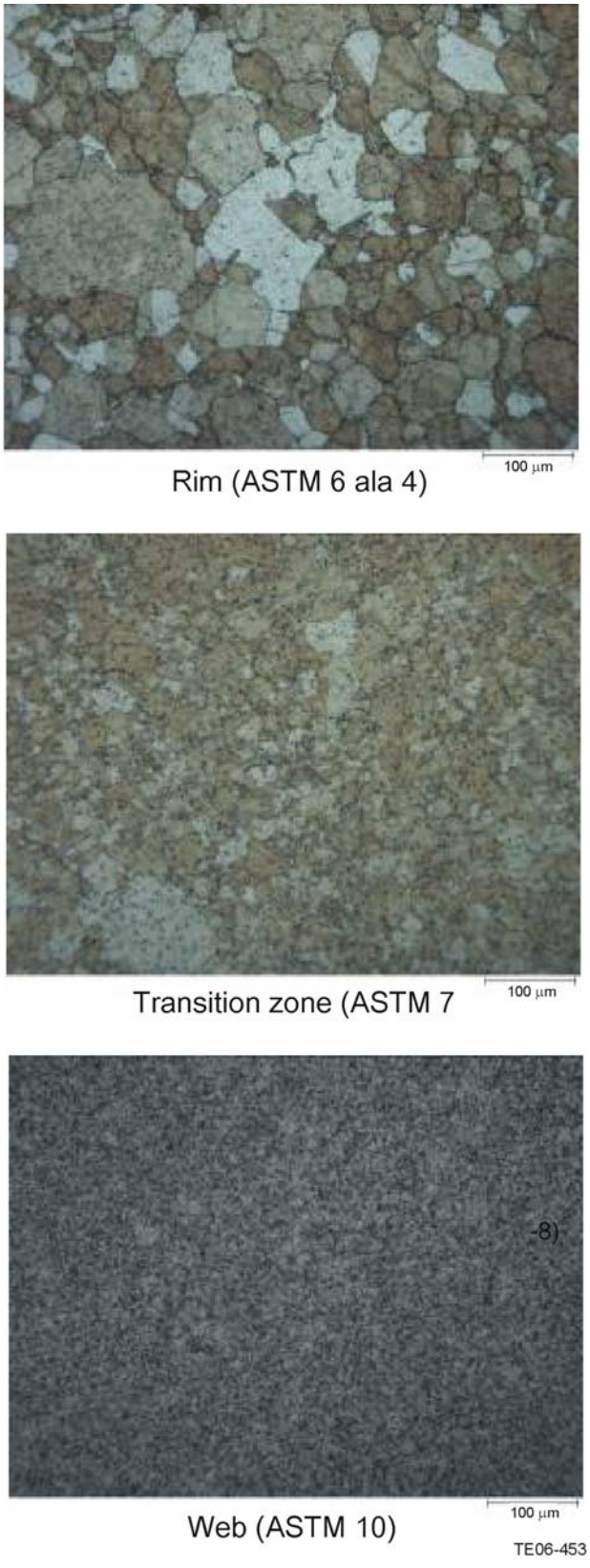

Figure 11. Microstructure of DMHT Disk Showing Coarse Grain in Rim (Left), Medium Grain in Transition Zone (Center), and Fine Grain in Web (Right).

2.2 WE 2—Disk Machining, Instrumentation, and Spin Test Definition

2.2.1 Disk Machining

Ladish forged, heat-treated, and machined the Alloy-10 forgings to the 'square cut' shape shown in Figure 12. While still at Ladish, the 'square cut' disks passed ultrasonic inspection. The disks were then shipped to GE's machining supplier, Douglas Machine, for finish machining.

Although finish machining was a GEAE task, AADC coordinated with GEAE and the machining subcontractor during the process. After machining, the disks were shipped to AADC for inspection. Following inspection, AADC shipped the disks to Test Devices, Inc. for spin testing.

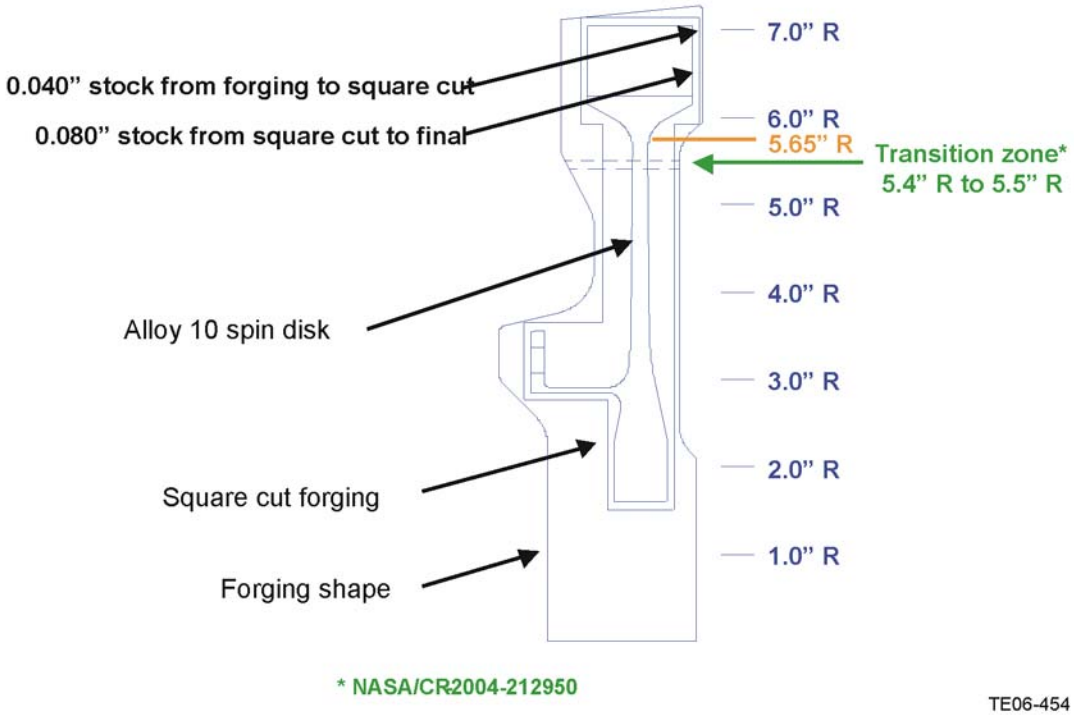

Figure 12. Disk Machining Geometry.

2.2.2 Instrumentation

Selection and positioning of instrumentation was a group decision driven by the intent to measure stresses in the transition zone at burst. The number of strain gages selected was constrained by budget. Instrumentation locations proposed by AADC are illustrated in Figure 13. The details and location numbers assigned by AADC and Test Devices, Inc. are provided in Table 2. The locations primarily correspond to the locations of maximum tangential strain

(bottom of rim hole), biaxial stress (in the web just above and just below the transition) and of high tangential strain in the bore of the wheel.

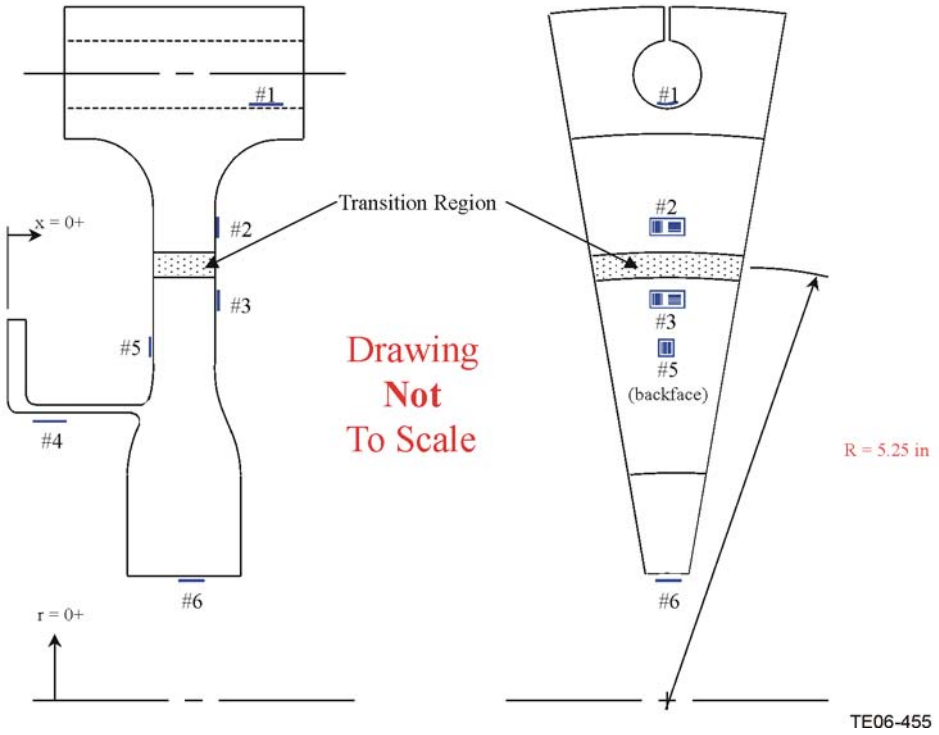

Figure 13. Proposed Locations for Strain Gages.

TABLE 2. STRAIN GAGE DESIGNATION AND LOCATION.

Location #		Micro Measurements Designation	Strain Measured	Location	
AADC	Test Devices			x (inches)	r (inches)
1	1, 9	062AQ-1X	max tangential strain	1.83	bottom of through hole
2	2, 3	062TT-1X	web radial and tangential strain (supersolvus region)	flat (non-hub) face of web	mean transition zone radius + 0.25" (~ 5.5")
3	4, 5	062TT-1X	web radial and tangential strain (subsolvus region)	flat (non-hub) face of web	mean transition zone radius - 0.25" (~ 5.0")
4	6	062AQ-1X	max axial strain	0.185	ID of load transfer hub
5	n/a	062AQ-1X	max radial strain	hub face of web	3.53
6	8, 10	062AQ-1X	Tangential strain in bore	1.23	ID of bore
7	1, 9	062AQ-1X	duplication of (1)	1.83	bottom of through hole
8	2, 3	062AQ-1X	duplication of (6)	1.23	ID of bore

2.2.3 Spin Test Definition

The objective of the spin testing was to burst the disks. With that goal, the disks were designed to burst within the operating range of the selected spin pit. To predict a burst speed, effort was expended investigating a new failure criteria for the wheel based on results of the elastic-plastic analysis, which will be discussed in Section 2.3.

A three-cycle test procedure was developed and proposed. Cycle 1 called for ramping the speed up to 20,000 rpm and back down to 0 rpm for both wheels. The 20,000 rpm speed, corresponding to the end of the linear elastic regime, was intended to make sure all instrumentation was working properly. The second cycle called for ramping up to 25,000 rpm for the DMHT wheel and 25,500 rpm for the subsolvus wheel and then ramping back down to 0 rpm in both cases. These speeds, corresponding to between 0.15 and 0.20 inches in total radial displacement, were intended to take the wheel into the plastic regime. By decelerating back down to rest, the plastic portion of the radial displacement could be measured. The predicted or expected radial rim displacement is illustrated in Figures 14 and 15. The third cycle called for ramping the speed back up until disk failure was achieved. This was predicted to be ~25,250 rpm for the DMHT wheel and ~26,000 rpm for the subsolvus wheel.

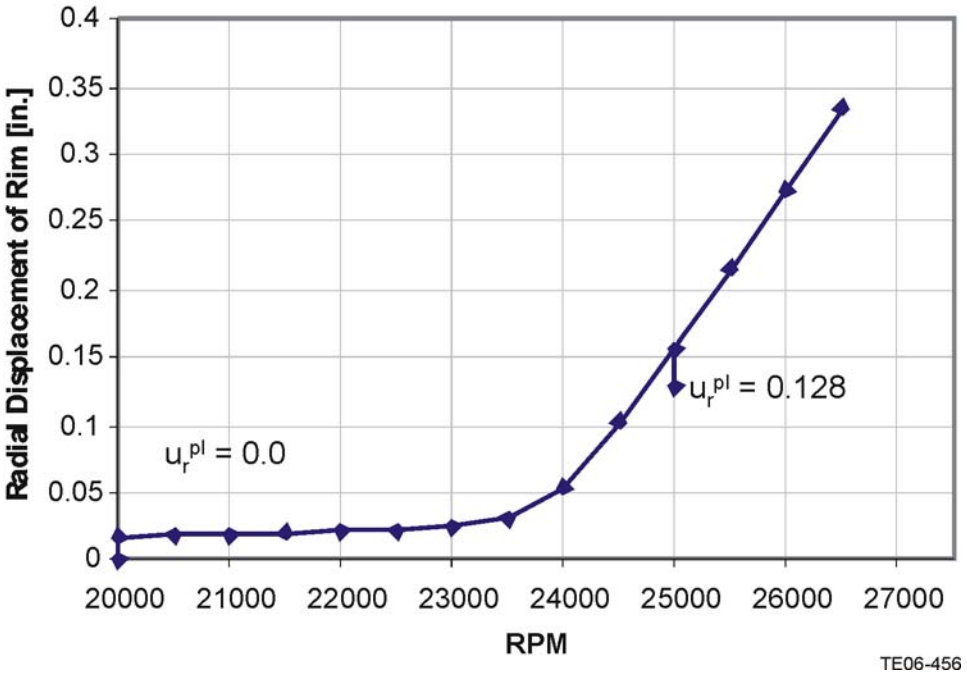

Figure 14. Radial Displacement of DMHT Rim (No Hysteresis Effect Modeled).

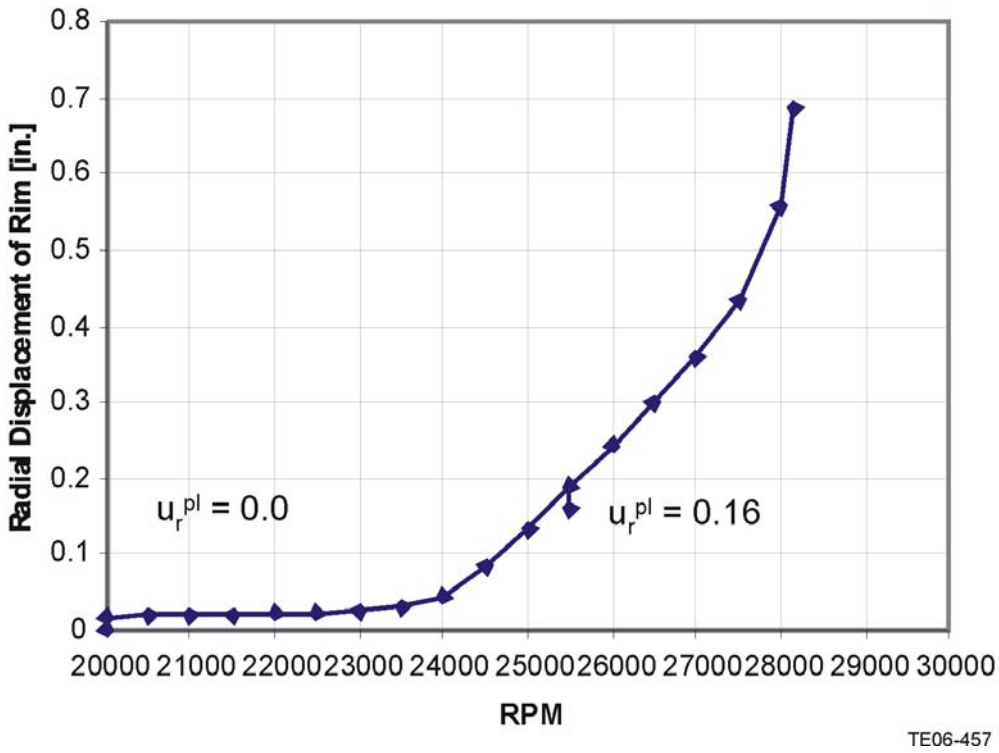

Figure 15. Radial Displacement of Subsolvus Rim (No Hysteresis Effect Modeled).

The actual test procedure run was modified slightly from what was originally proposed. The top speed of cycle 1 was increased to 21,000 rpm to take the wheels slightly into the plastic regime. The criteria for top speed in cycle 2 were changed to correspond to a strain gage reading of 0.03 (maximum the gage is certified for) at the base of the rim hole. The test plan is presented in a step-by-step format in the following:

- Final Spin Test Plan
  - Cycle 1
    - Ramp speed to 21,000 rpm
    - Decelerate speed to 0 rpm
    - Measure permanent radial displacement
  - Cycle 2
    - Ramp speed to achieve a strain gage reading of 0.03 at the base of the rim hole
    - Decelerate speed to 0 rpm
    - Measure permanent radial displacement
  - Cycle 3
    - Ramp speed until disk failure

2.3 WE 3—Characterize Static and Cyclic Disk Behavior and Predict Spin Pit Behavior of Disks

2.3.1 Characterize Static and Cyclic Disk Behavior

The mechanical test plan was designed to cover two needs:

- Tensile testing to determine true stress—true strain response in the fine grain, coarse grain, and transition zone sections of the forging
- Low cycle fatigue (LCF) testing to verify the transition zone does not represent a plane of weakness in cyclic operation

The tensile test plan included smooth specimens to generate the stress-strain curves and notched specimens that would be used to validate the deformation and fracture models using triplicate testing for each configuration. Specimens were extracted from the fine grain bore, transition zone, and coarse grain rim. These specimens all were taken from the chordal direction. The LCF test plan constituted six tests each from the fine grain, transition zone, and grain regions. The fine grain and coarse grain specimens were extracted from the chordal direction, while the transition zone specimens were oriented radially with the transition zone designed to be in the center of the gage section. Figure 16 shows the specimen blanking (cut-up) diagram employed for the testing program. The specimen blanking was conducted using saw cutting, and it proved to be quite difficult to maintain saw alignment. A lesson learned from this experience is that the more expensive electrodischarge machining (EDM) wire blanking is required for this material and thickness combination.

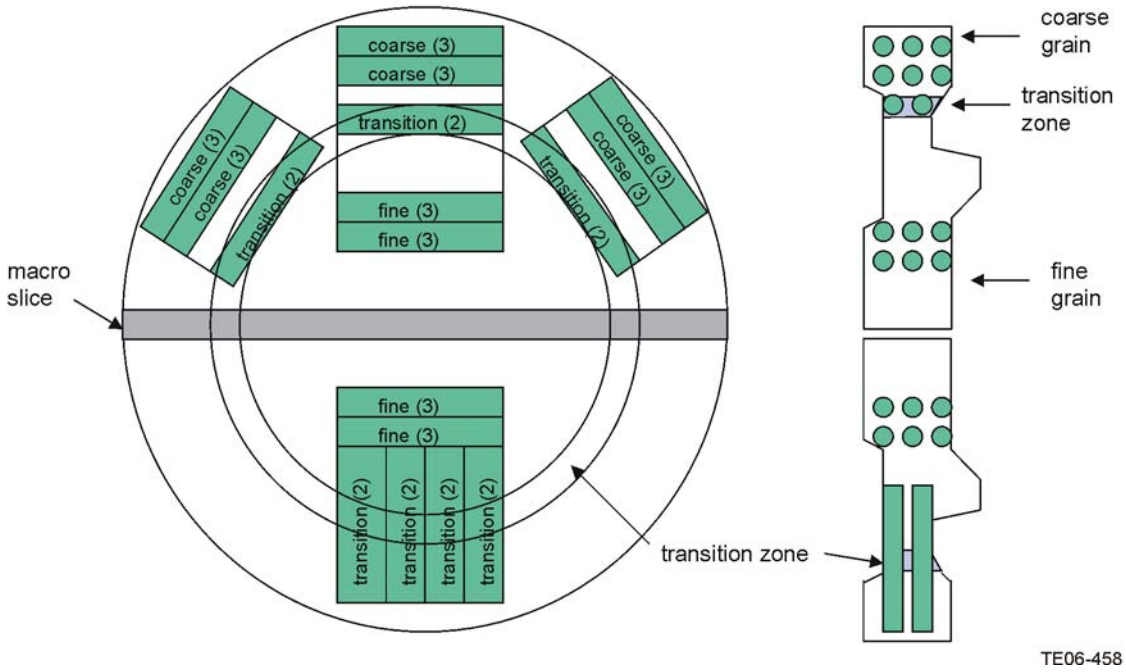

Figure 16. Specimen Blanking Diagram for DMHT Alloy 10 Disk.

The specimen machining and testing was conducted by Mar-Test, Inc. The tensile testing was conducted using extensometry through specimen failure. The extensometry data were fed to two X-Y recording charts for each smooth bar test. The first chart covered the low strain range data and was used to determine modulus and yield strength. The second chart covered the full strain history to failure. The smooth bar tensile test results are summarized in Table 3. The load-extension data were converted to true stress-true strain. The true strain was partitioned into elastic and plastic components. Various forms of equations were used to fit the plastic strain data to the true stress. A hyperbolic tangent equation provided an excellent fit except for the very start of plasticity and this equation form was selected to perform the subsequent analyses. Figure 17 shows a representative curve fit. Table 3 also includes the calculated values for true stress and true strain at fracture. The true stress-true strain curves for specimens AF4, BT2, and CC4 were selected to represent the fine grain, transition zone, and coarse grain regions, respectively, for the subsequent finite element modeling activity.

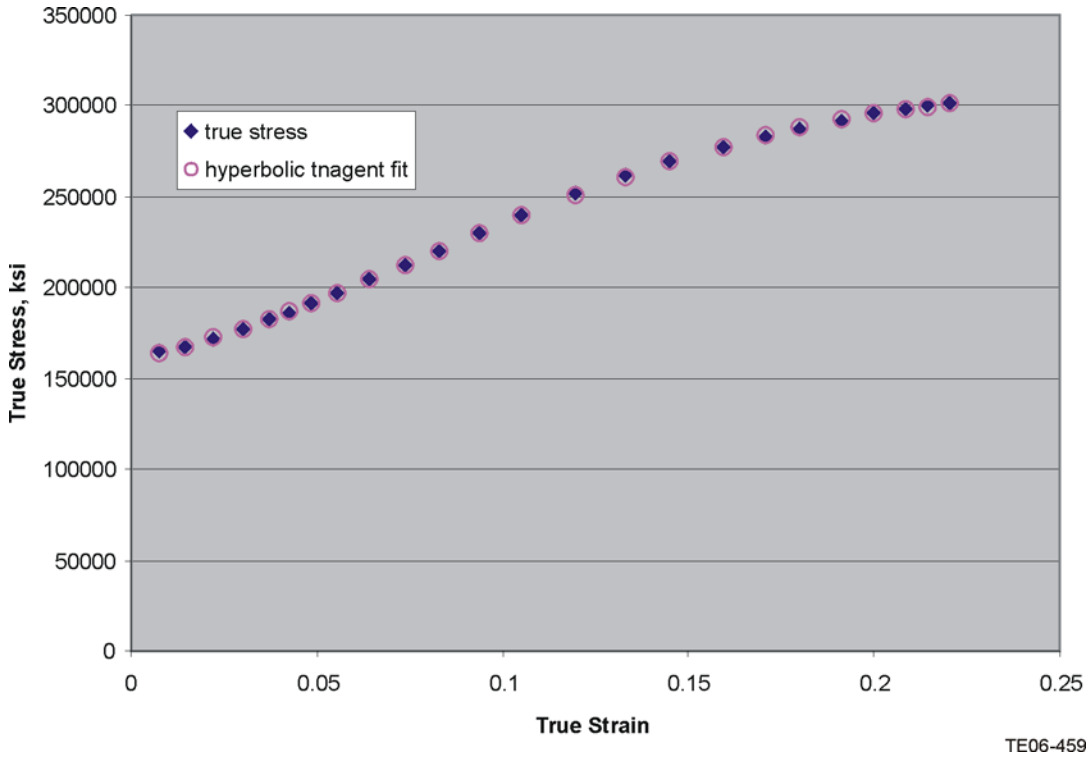

Figure 17. Calculated True Stress-True Strain Behavior for Smooth Tensile Specimen AF4 and Best Fit Hyperbolic Tangent Curve.

The notched bar specimen configuration constituted a circumferentially notched round bar with a 0.25-in. nominal gage diameter, a 0.18-in. notch root diameter, and a theoretical stress concentration factor of 3.45. A 0.5-in. long gage length extensometer was centered about the notch to monitor elongation to specimen failure. The notch tensile test results are summarized in Table 4. The load/extension data from these tests were furnished to the AADC structural analyst to calibrate the Alloy 10 deformation behavior models and fracture criteria prior to conducting the finite element model simulation of the disks.

A simplified elastic-plastic failure criteria was proposed wherein fracture occurs when the local maximum principle true stress exceeds a critical value. It was recognized that this simplified theory neglects short crack formation behavior such as stage 1 crystallographic cracking from concentrated slip within favorably oriented grains, the slow growth and linkage of these cracks to a critical size, and the geometric and external loading influences on these phenomenon.

TABLE 3. ROOM TEMPERATURE SMOOTH BAR TENSILE RESULTS.

Specimen I.D.	Modulus 10^6 psi	0.2% yield strength, ksi	Ultimate tensile strength, ksi	Area reduction, %	Elongation, %	True fracture strain, %	True fracture stress, ksi	Foot Note Ref
Fine Grain								
AF4	32.7	163	240	23	25	22.03	301992	IX, 1
AF5	35.2	163	240	27	25	21.83	298331	IX, 1
BF4	30.1	164	240	23	24	22.90	302100	IX, 1
Average	32.7	163.3	240	24.3	24.7	22.25	300808	
Transition Zone								
AT4	37.2	165	243	27	25	Extensometer slipped		OX, 1
AT5	31.3	166	240	26	21	18.04	262646	OX, 1
BT2	31.2	160	233	26	26	21.33	289095	IX, 1
Average	33.2	163.7	238.7	26.3	24	19.69	275871	
Coarse Grain								
CC4	27.8	159	227	26	25	23.14	284685	IX, 1
CC5	28.9	153	225	19	24	24.41	288232	OX, 2
DC4	27.6	160	226	20	18	18.14	270209	OX, 2
Average	28.1	157.3	226	21.7	22.3	21.9	281042	

IX: Failed inside of extensometer probes
OX: Failed outside of extensometer probe in the test section
1: Elongation calculated from change in length between gage marks = 1 inch
2: Elongation calculated from change in overall length, using adjusted gage length of 1.236 inches

TABLE 4. ROOM TEMPERATURE NOTCHED BAR TENSILE RESULTS.

Specimen I.D.	Load deflection slope, KIPS/in.	Ultimate tensile strength, ksi	0.001 inch offset yield strength, ksi	Overall length change, in.
Fine Grain				
AF6	57.3	273	247	0.012
BF5	60.8	269	247	0.011
BF6	59.6	274	255	0.011
Average	59.2	272	249.7	0.0113
Transition Zone				
AT6	57.1	268	246	0.012
CT2	55.4	266	246	0.012
DT2	62.7	272	256	0.013
Average	58.4	268.7	249.3	0.0123
Coarse Grain				
CC6	56.4	265	243	0.012
DC5	56.0	257	235	0.013
DC6	59.0	261	243	0.012
Average	57.1	261	240.3	0.0123

The LCF testing was conducted at 1200°F with smooth specimens ($K_t = 1$) under R = 0 (zero to maximum) loading conditions. All tests were performed under load control. The stress levels were selected to provide an aim life of approximately 20,000 cycles in the fine grain material. A 170-ksi stress range was selected for the first three specimens, which produced higher lives than desired. The stress range was increased to 180 ksi and the remaining specimens were tested using this range. The test results are provided in Table 5.

As expected, the coarse grain LCF capability is significantly lower than the fine grain material. Contrary to expectations, the transition zone material was equal or superior to the fine grain material. Past work by NASA showed that the transition zone LCF capability generally tracked with the coarser grain lives. NASA performed metallographic and fractographic examinations on the failed test specimens. It was concluded that some of the specimens with chordal orientation that were intended for tensile testing were transposed with the radially oriented LCF specimens. It was also shown that the radial specimens were somewhat biased towards the fine grain material. The web material had a faster cooling rate from solution heat treatment than the thicker bore section, and presumably, this provided sufficient fatigue life enhancement to offset the somewhat coarser grain size in the specimens tested.

TABLE 5. 1200°F R = 0 SMOOTH BAR LOW CYCLE FATIGUE RESULTS FROM DMHT PROCESSED ALLOY 10 FORGING.

Specimen I.D.	Stress range, ksi	Cycles to crack initiation	Cycles to failure	Failure location
Fine Grain				
AF3	170	N/A	>58524	Adaptor failure
AF1	180	8531	8694	IX
AF2	180	15026	15281	IX
BF1	180	5628	6050	IX
BF2	180	10963	11095	IX
BF3	180	32187	32187	IX
Average for 180 ksi tests		14467	14661	
Transition Zone				
DT1	170	N/A	>75580	Threads
AT1	180	12555	12774	IX
AT2	180	17603	17889	IX
AT3	180	18550	18680	OX
BT1	180	13582	13916	IX
CT1	180	27943	28352	IX
Average for 180 ksi tests		18047	18332	
Coarse Grain				
CC1	170	3788	4097	OX
CC2	180	1235	1463	IX
CC3	180	2498	2918	IX, MI
DC1	180	2968	3148	IX
DC2	180	2002	2415	IX
DC3	180	1294	1740	IX
Average for 180 ksi tests		1999	2337	

N/A: Not available.

IX: Failed inside of extensometer probes.
OX: Failed outside of extensometer probe in the test section.
MI: Multiple initiations.

2.3.2 Predict Spin Pit Behavior

The initial predicted burst rpm were reported as:

- 25,250 rpm for the DMHT wheel
- 26,000 rpm for the subsolvus wheel

The burst speeds were calculated by equating the maximum plastic strain in the notched specimen at failure to that occurring in the spinning wheel. The maximum plastic strain occurred

at the base of the rim hole. The wheel was predicted to burst when the maximum strain during spin testing reached the -3σ maximum plastic strain that occurred in the notched specimen at failure. The predicted failure rpm is shown as the intersection of -3σ strain at failure and strain predicted at rpm in Figures 18 and 19.

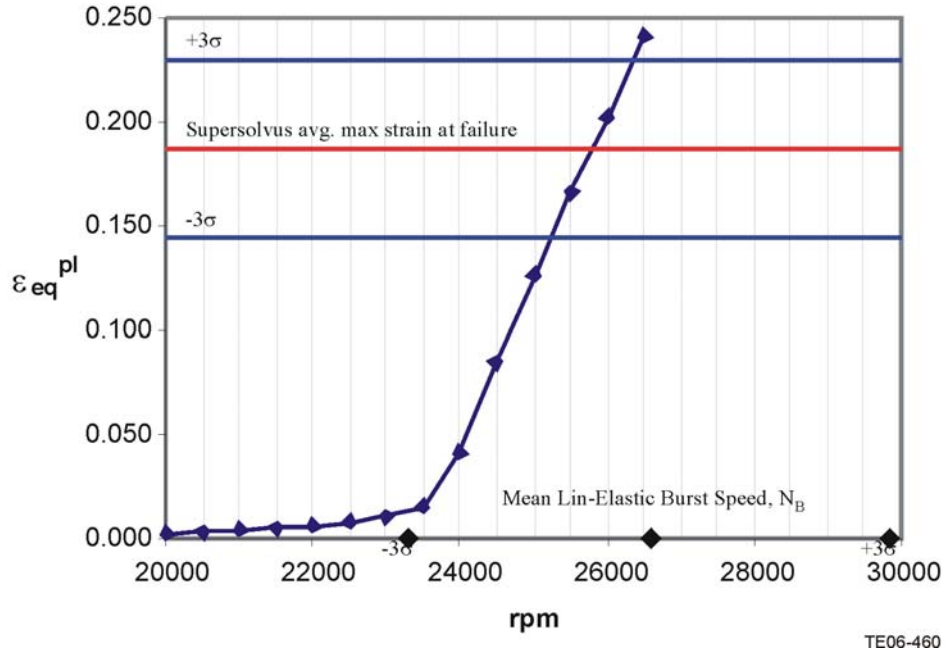

Figure 18. Maximum Equivalent Plastic Strain in DMHT Wheel.

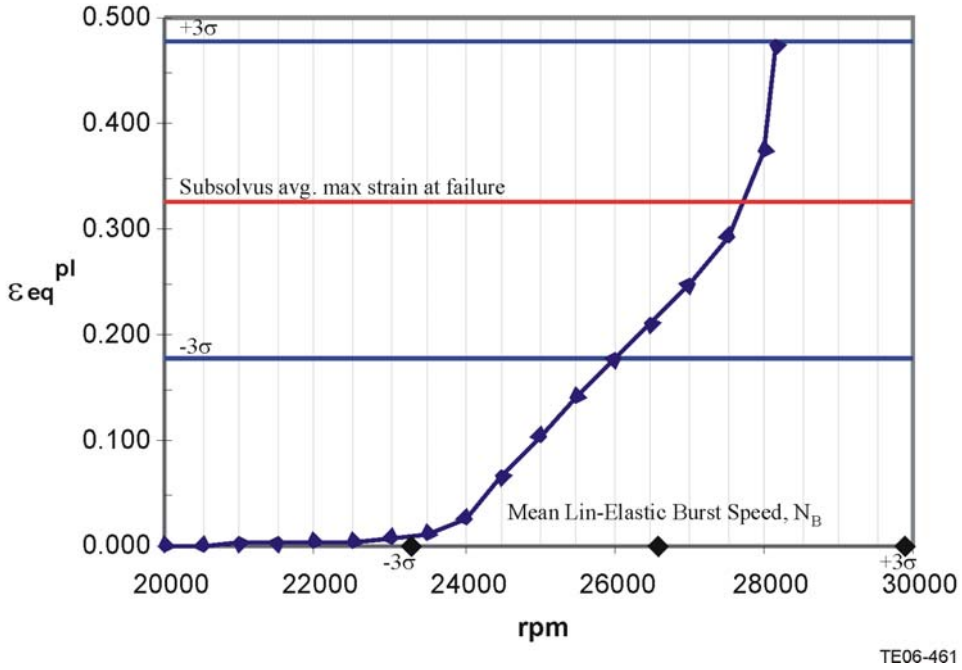

Figure 19. Maximum Equivalent Plastic Strain in Subsolvus Wheel.

To predict a burst speed, effort was expended investigating a new failure criteria for the wheel based on results of the elastic-plastic analysis. To support this work, notched specimens were tested and analyzed. The smooth tensile specimen data used to calibrate the predicted elastic-plastic strain versus stress are shown in Figure 20. The nonlinear elastic-plastic behavior was modeled by including tabular input of the true stress-logarithmic strain response of the material obtained from representative smooth bar tensile tests.

FEA predictions of the stress/strain state present in the notched tensile specimens at failure used to postulate the failure state for the wheel are shown in Table 6.

TABLE 6. FEA PREDICTIONS OF MAXIMUM STRAINS PRESENT AT FAILURE IN NOTCHED SPECIMENS.

	Test Specimen	total engineering longitudinal strain, $(\varepsilon_L)_{eng}$	total logarithmic longitudinal strain, $(\varepsilon_L)_{ln}$	plastic longitudinal engineering strain, $(\varepsilon_L^{pl})_{eng}$	plastic equivalent strain, ε_{eq}^{pl}
SUBSOLVUS	AF6	0.3097	0.3098	0.3004	0.3368
	BF5	0.2542	0.2545	0.2449	0.2748
	BF6	0.3420	0.3422	0.3328	0.3738
	Average	0.3020	0.3022	0.2927	0.3285
	St Dev	0.0444	0.0443	0.0445	0.0500
	C.O.V.	0.1471	0.1468	0.1519	0.1523
TRANSITION	AT6	0.3098	0.3101	0.3005	0.3376
	CT2	0.2533	0.2536	0.2441	0.2739
	DT2	0.1332	0.1332	0.1249	0.1408
	Average	0.2321	0.2323	0.2232	0.2508
	St Dev	0.0902	0.0904	0.0897	0.1004
	C.O.V.	0.3886	0.3889	0.4017	0.4004
SUPERSOLVUS	CC6	0.1868	0.1874	0.1777	0.1998
	DC5	0.1612	0.1615	0.1524	0.1716
	DC6	0.1776	0.1781	0.1686	0.1897
	Average	0.1752	0.1757	0.1662	0.1870
	St Dev	0.0130	0.0131	0.0128	0.0143
	C.O.V.	0.0740	0.0747	0.0771	0.0764

The initial failure hypothesis is based on equating the maximum plastic strain in the notched specimen at failure to that occurring in the spinning wheel. FEA of the wheel was used to predict the rotational speed necessary to achieve this failure state in the spinning wheel. Based on these

analyses, the maximum plastic strain in the wheel was found to occur at the base of the rim hole as designed (Figures 21 and 22).

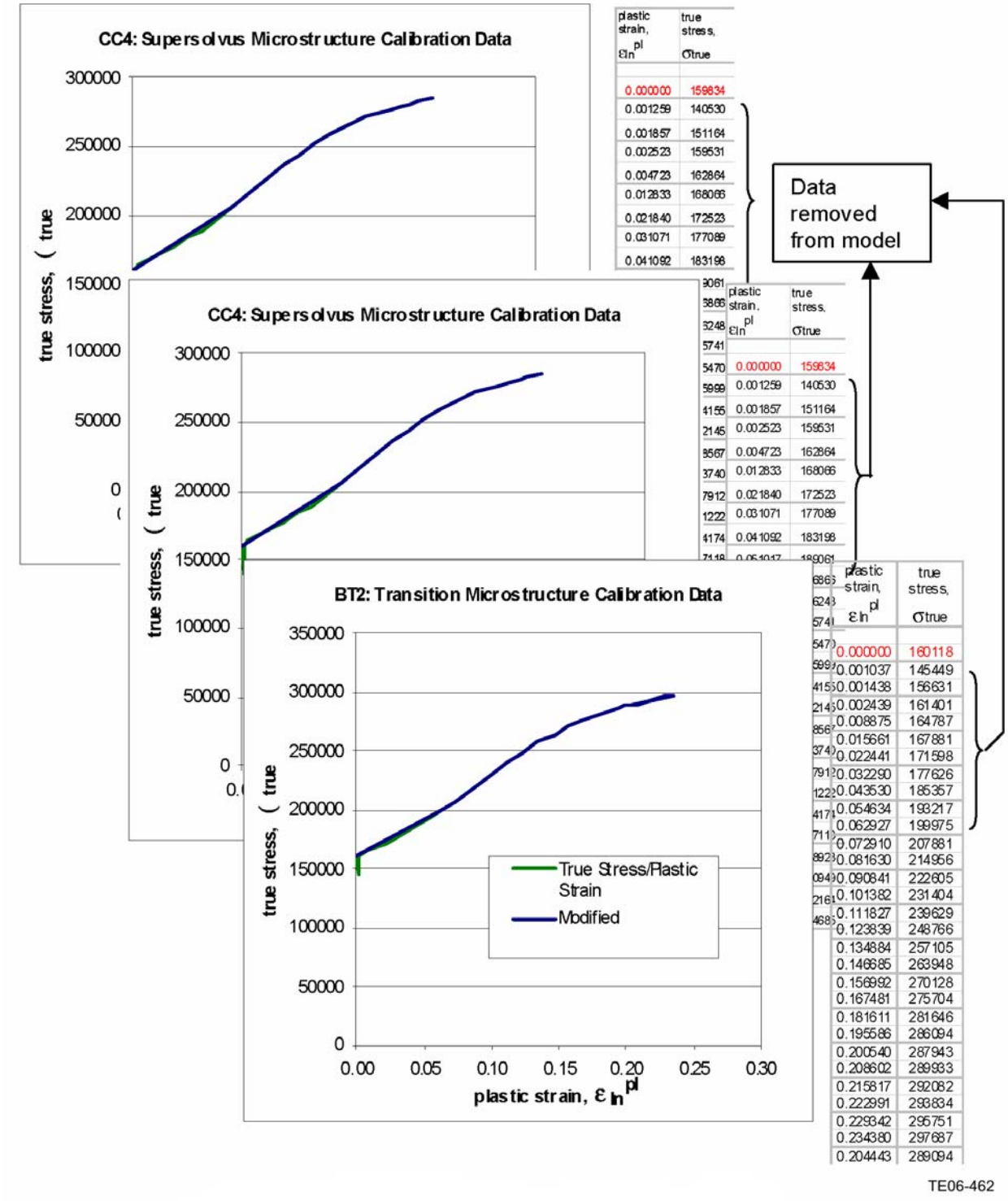

Figure 20. Smooth Tensile Specimen Data.

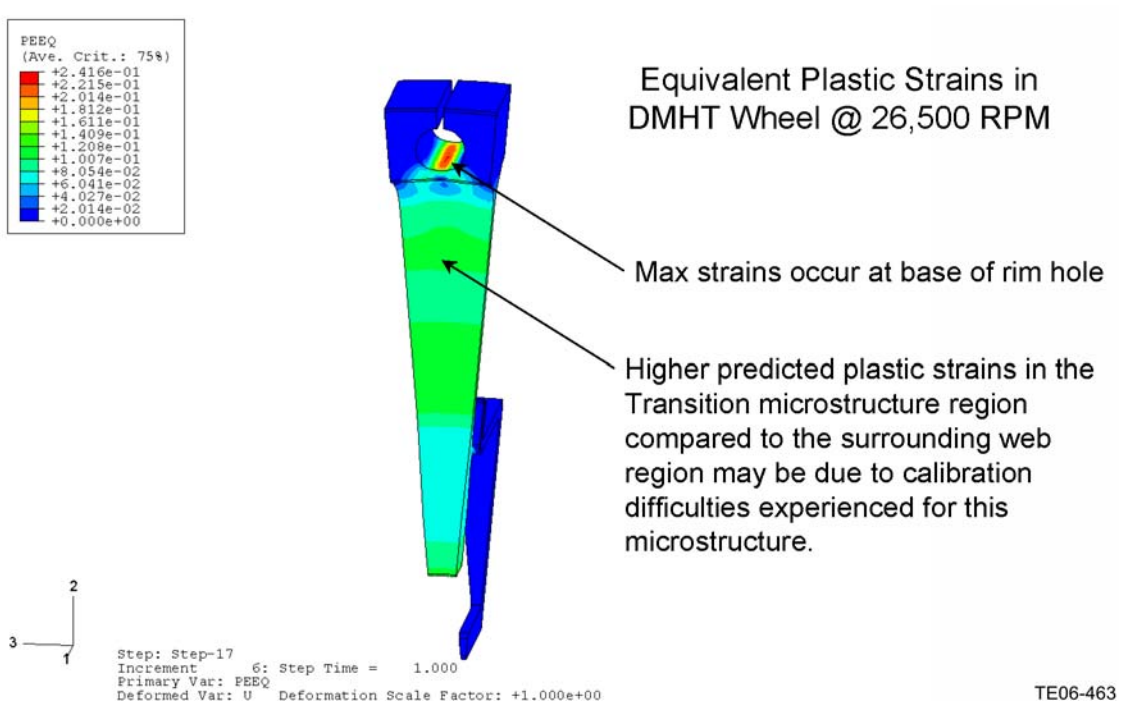

Figure 21. Calculated Maximum Plastic Strain in Disk.

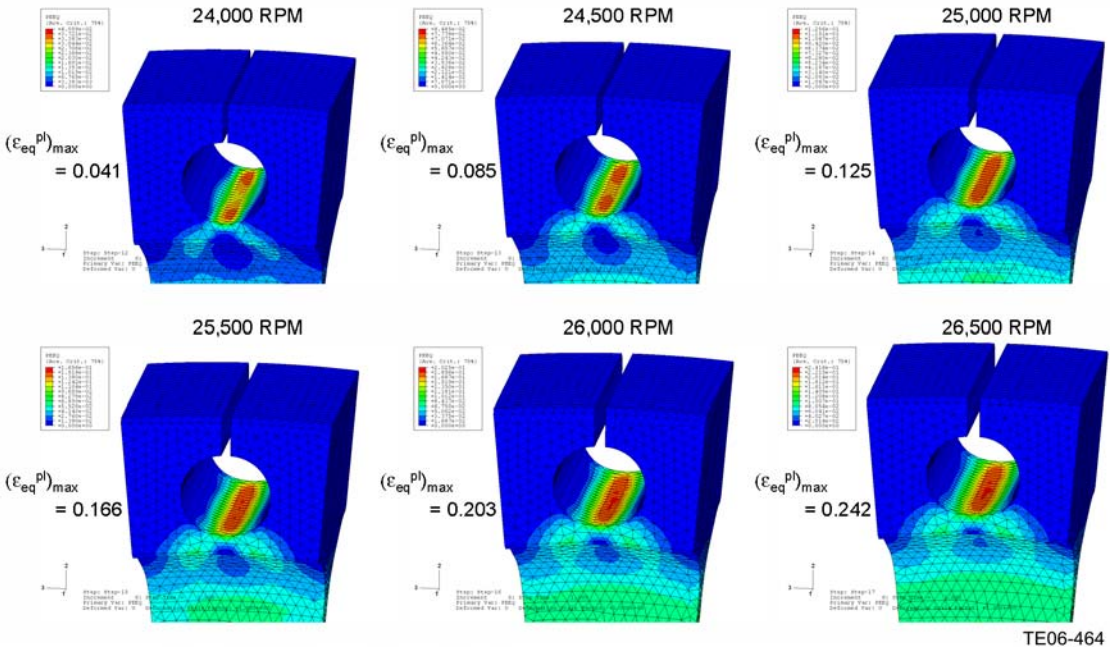

Figure 22. Evolution of Peak Equivalent Plastic Strain in DMHT Wheel.

2.4 WE 4—Analyze Spin Test Data

2.4.1 Initial Analysis Predicted Versus Actual Burst rpm

Mixed results were achieved upon running the tests and comparing the actual results to the predicted behavior. First, the burst speed was significantly overpredicted. The actual measured

burst speeds for the two wheels were 24,005 (DMHT) and 24,228 rpm (subsolvus). However, favorable results were found when comparing the predicted and measured strain response as a function of rotational speed (Figures 23, 24, and 25). The burst crack initiation site also matched the peak, model predicted strain location at the wheel's last continuous fiber occurring at the base of the rim hole. In light of this, it became obvious that while the current failure criterion was in error, the fact that the material state could accurately be predicted into the plastic regime was reason to believe that with a properly formulated failure criterion, accurate burst speed predictions could be achieved.

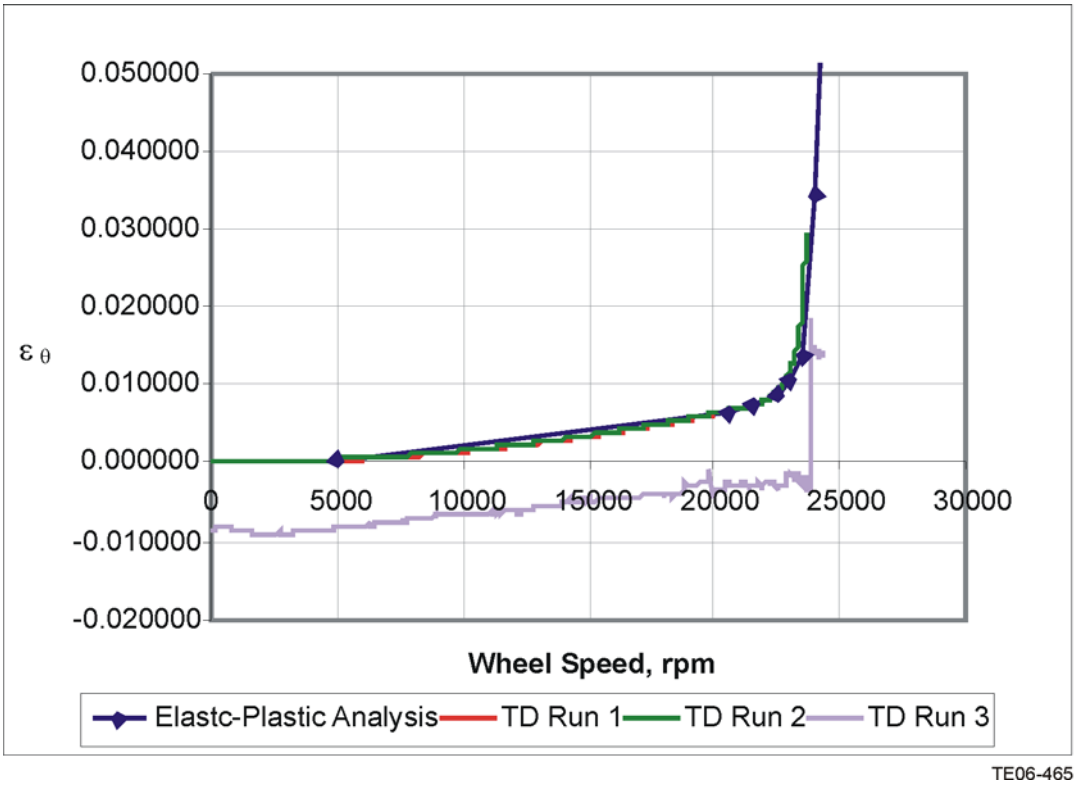

Figure 23. FEA Prediction of Strain Present in DMHT Wheel at Gage No. 1/1 Location—Bottom of Through-hole.

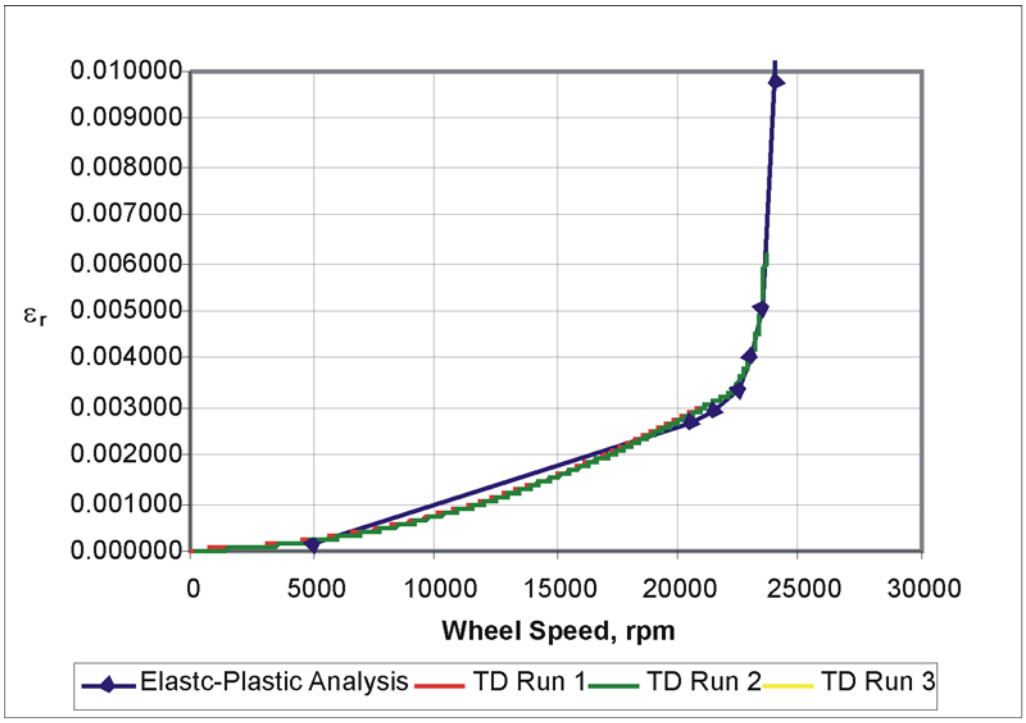

Figure 24. FEA Prediction of Strain Present in DMHT Wheel at Gage No. 2/2 Location—in Transition Zone Area.

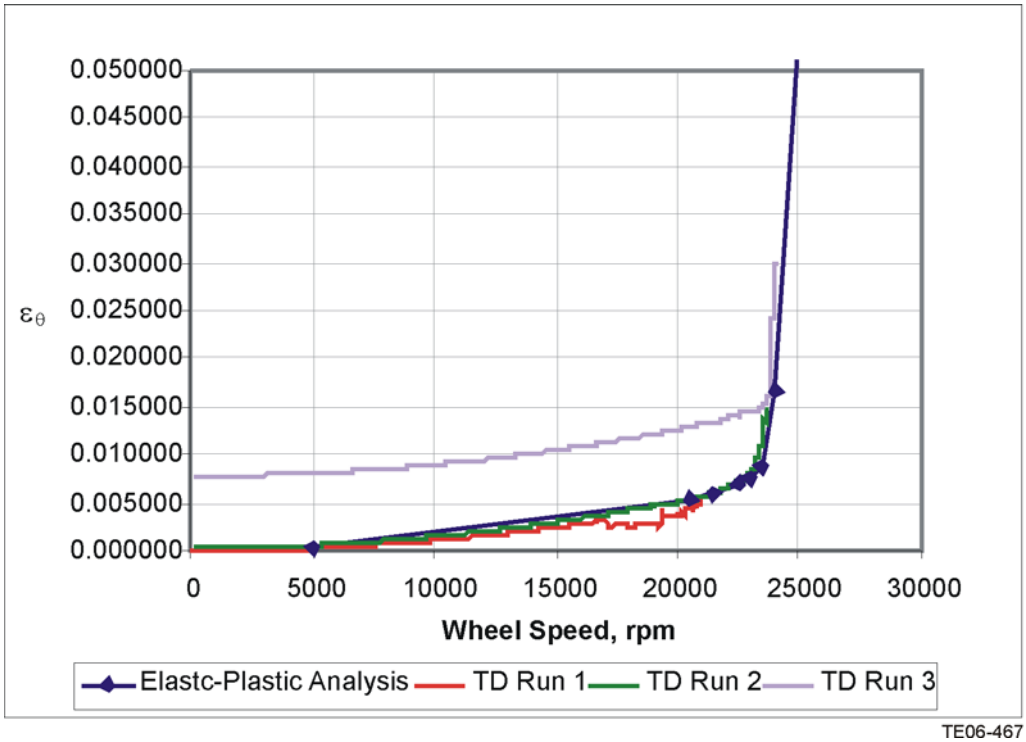

Figure 25. FEA Prediction of Strain Present in DMHT Wheel at Gage No. 6/8 Location—Bore I.D.

2.4.2 Additional Analysis of Predicted Versus Actual Burst rpm

As a result of the previously sited, overpredicted burst speed, the material correlation and prediction methodology were revisited. In initially modeling the failure state of the notched specimen, the recorded load at failure had been applied to the finite element model, and the resulting stress/strain state was utilized in formulating the failure criteria. During experimental testing of the notched specimens, the extensometer elongation at failure had also been recorded. Upon review, it was found the FEA prediction for the displacement corresponding to the specified failure load exceeded the observed elongation. The slope of the force versus displacement curve is very low as failure is approached. This leads to large changes in both the observed and predicted displacements for very small changes in load. Therefore, to reduce the sensitivity of the predicted stress/strain state at failure to possible experimental errors, it was decided to recorrelate the failure of the notched specimen utilizing the recorded displacement at failure rather than load at failure. Checking the resultant force in the FEA and comparing to the experimentally observed failure load found only a slight discrepancy.

The change made to the prediction methodology was to base the failure upon stress rather than plastic strain. In both the notched specimen and the wheel, plastic yielding occurred in isolated regions surrounded by material behaving linear elastically. Consequently, the observed plastic strain states at failure in both cases were not allowed to develop freely. The new criterion proposed was to compare the maximum axial tensile stress in the notched specimen to the maximum hoop stress in the wheel. This is effectively the maximum principal stress criterion referenced in Section 2.3.1 (see Table 7 for listing of calculated stress by type). The axial stress at fracture in the notched specimens from Table 7 correlates very well with the true fracture stress in the smooth tensile specimens from Table 3, supporting the maximum principal stress criterion.

TABLE 7. FEA PREDICTIONS OF MAXIMUM STRESSES PRESENT AT FAILURE IN NOTCHED SPECIMENS.

	Test Specimen	axial stress, σ_y [ksi]	radial stress, σ_x [ksi]	Mises stress, σ_{Mises} [ksi]
SUBSOLVUS	AF6	305.6500	133.0300	187.0700
	BF5	305.9000	133.1300	187.3100
	BF6	299.0100	127.3600	181.9100
	Average	303.5200	131.1733	185.4300
	St Dev	3.9078	3.3028	3.0508
	C.O.V.	0.0129	0.0252	0.0165
SUPERSOLVUS	CC6	286.2400	117.8300	179.3500
	DC5	293.4200	123.6200	183.0200
	DC6	278.5900	111.2100	176.4700
	Average	286.0833	117.5533	179.6133
	St Dev	7.4162	6.2096	3.2829
	C.O.V.	0.0259	0.0528	0.0183

The predicted burst speeds based on the two elastic-plastic methodologies discussed in this report versus an empirically based methodology utilizing linear elastic finite element stress models are presented in Table 8. All three models overpredicted the burst speeds to some extent, but the elastic-plastic maximum principal stress model was considerably closer for both the DMHT and subsolvus wheels.

TABLE 8. PREDICTED VERSUS ACTUAL BURST SPEED USING THREE BURST CRITERIA.

	Burst speed				Percent error		
		Predicted (based on average properties)			Predicted burst rpm/actual		
Wheel	Actual	Empirical linear elastic stress	Elastic-plastic maximum plastic strain	Elastic-plastic maximum principal stress	Empirical linear elastic stress	Elastic-plastic maximum plastic strain	Elastic-plastic maximum principal stress
DMHT	24,005	25,348	25,200	24,541	5.59	4.98	2.23
Subsolvus	24,228	26,121	26,000	24,866	7.81	7.31	2.63

NASA performed fractographic examination of the failed wheels and identified numerous surface initiated small cracks at the base of the intact rim holes from the burst wheel fragments. Upon the onset of plastic yielding, the location of maximum hoop stress moved below the surface. The location of maximum hoop stress at the failure speed was approximately 0.125 inches below the surface, as shown in Figure 26. Thus, it would appear that maximum hoop stress could not be the cause of crack initiation.

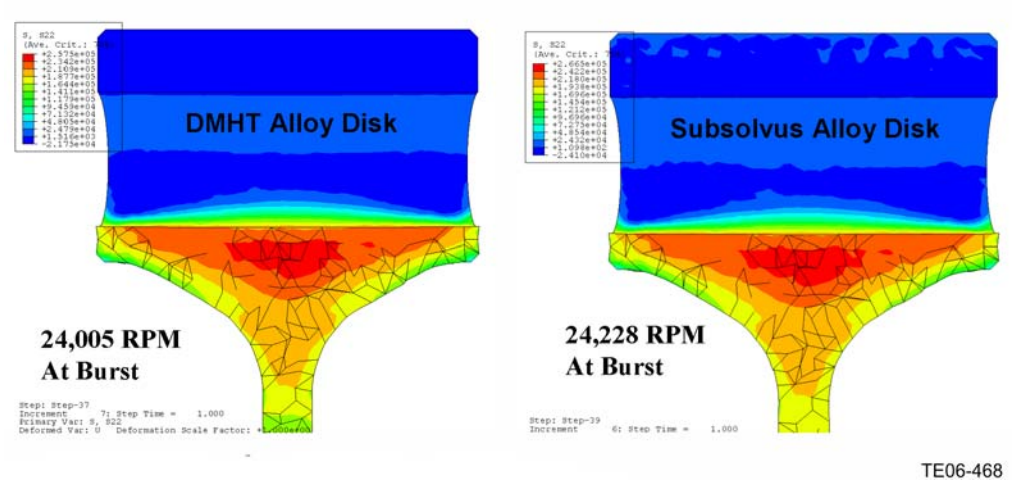

Figure 26. Location of Maximum Hoop Stress.

Further examination of the results of the analysis found that the von Mises stress was, in fact, a maximum in the regions where high surface crack densities occurred (Figure 27). These observations suggest that concentrated slip behavior and crack formation mechanisms need to be determined to develop an accurate physics based burst criterion.

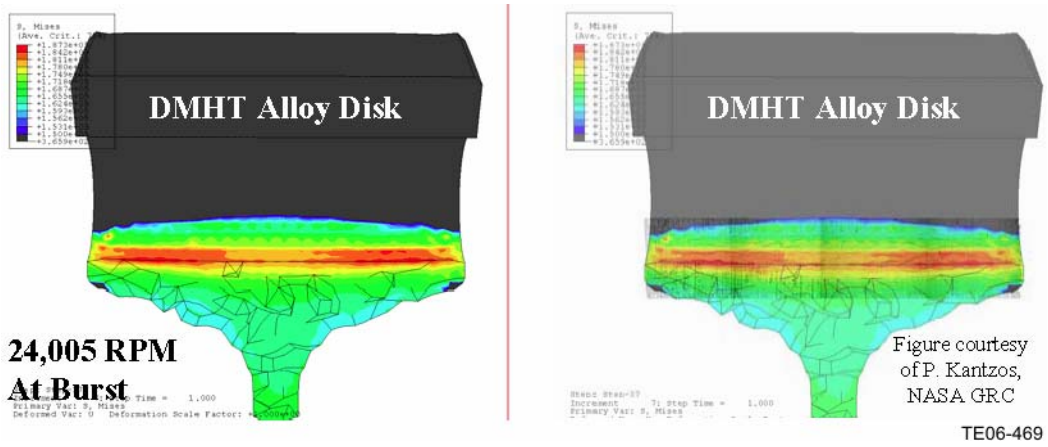

Figure 27. Von Mises stress contours without (left) and with (right) overlay of crack locations.

3. Summary and Recommendations

This project enabled the validation of the design methodology to predict the behavior of dual grain structure near the burst limit. This achievement is a critical milestone in the implementation of DMHT technology into future turbine rotors.

While this project and previous research furthered the understanding of advanced nickel disk alloys and processes, the technology must move forward on several fronts. The following additional work is recommend to enable DMHT transition to the commercial sector:

- DMHT rotor burst tests at high rim temperatures to further correlate analytical predictions.
- Model and simulate the microstructural evolution using software codes such as PreciCalc™ and DEFORM™. This would provide a better understanding of the mechanical behavior interactions in highly stressed disk features such as rim attachments.
- Investigate material corrosion behavior at high rim temperatures.
- Extension of probabilistic lifing methodologies to the DMHT processed powder metallurgy alloys.

REPORT DOCUMENTATION PAGE

Form Approved
OMB No. 0704-0188

1. AGENCY USE ONLY (*Leave blank*)	2. REPORT DATE	3. REPORT TYPE AND DATES COVERED
	May 2006	Final Contractor Report

4. TITLE AND SUBTITLE

Spin Testing of Superalloy Disks With Dual Grain Structure

5. FUNDING NUMBERS

WBS 698259.02.07.03
NAS3–01143, Task 4

6. AUTHOR(S)

Tab M. Heffernan

7. PERFORMING ORGANIZATION NAME(S) AND ADDRESS(ES)

Rolls-Royce North American Technologies, Inc.
P.O. Box 7162
Indianapolis, Indiana 46207

8. PERFORMING ORGANIZATION REPORT NUMBER

E–15574

9. SPONSORING/MONITORING AGENCY NAME(S) AND ADDRESS(ES)

National Aeronautics and Space Administration
Washington, DC 20546–0001

10. SPONSORING/MONITORING AGENCY REPORT NUMBER

NASA CR—2006-214338
EDR–90712

11. SUPPLEMENTARY NOTES

Project manager, John Gayda, Glenn Research Center, Materials and Structure Division, organization code RXA, 216–433–3273

12a. DISTRIBUTION/AVAILABILITY STATEMENT

Unclassified - Unlimited
Subject Category: 26

Available electronically at http://gltrs.grc.nasa.gov

This publication is available from the NASA Center for AeroSpace Information, 301–621–0390.

12b. DISTRIBUTION CODE

13. ABSTRACT ***(Maximum 200 words)***

This 24-month program was a joint effort between Allison Advanced Development Company (AADC), General Electric Aircraft (GEAE), and NASA Glenn Research Center (GRC). AADC led the disk and spin hardware design and analysis utilizing existing Rolls-Royce turbine disk forging tooling. Testing focused on spin testing four disks: two supplied by GEAE and two by AADC. The two AADC disks were made of Alloy 10, and each was subjected to a different heat treat process: one producing dual microstructure with coarse grain size at the rim and fine grain size at the bore and the other produced single fine grain structure throughout. The purpose of the spin tests was to provide data for evaluation of the impact of dual grain structure on disk overspeed integrity (yielding) and rotor burst criteria. The program culminated with analysis and correlation of the data to current rotor overspeed criteria and advanced criteria required for dual structure disks.

14. SUBJECT TERMS

Superalloy disks

15. NUMBER OF PAGES

42

16. PRICE CODE

17. SECURITY CLASSIFICATION OF REPORT	18. SECURITY CLASSIFICATION OF THIS PAGE	19. SECURITY CLASSIFICATION OF ABSTRACT	20. LIMITATION OF ABSTRACT
Unclassified	Unclassified	Unclassified	